Electronic Supplementary Information (ESI)

Engineering a ternary one-dimensional $Fe_2P@SnP_{0.94}@MoS_2$ mesostructure through magnetic field-induced self-assembly as high-performance lithium-ion battery anode

Jinyun Liu[a,*], Ting Zhou[a], Tianli Han[a], Liying Zhu[a], Yan Wan[a], Yunfei Hu[b,*], Zhonghua Chen[c,*]

Experimental

Chemicals: $FeCl_3·6H_2O$, urea, sodium hypophosphite ($NaH_2PO_2·H_2O$), trisodium citrate dehydrate, and $K_2SnO_3·3H_20$ were obtained from Aladdin. Tetraethyl silicate (TEOS) was purchased from Macklin. $NH_3·H_2O$, CH_4N_2S, $Na_2MoO_4·2H_2O$, and anhydrous ethanol were purchased from Sinopharm Chemical Reagent Co., Ltd. All chemicals were used directly without further purification.

Preparation of 1D $Fe_3O_4@SiO_2$: The Fe_3O_4 nanospheres were prepared by dispersing $FeCl_3·6H_2O$ (4.3 g), NaAc (4.0 g), and trisodium citrate dehydrate (1.0 g) in 70 ml of ethylene glycol. Then, a transparent solution was transferred into a Teflon-lined stainless steel autoclave and kept in an oven at 200 °C for 10 h. After that, the sample was collected, washed and dried. 0.05 g of Fe_3O_4 nanospheres were ultrasonically dispersed in 240 mL of anhydrous ethanol, and 30 mL of ammonia was added under a strong mechanical rate (800 rpm) for 10 min. Subsequently, 2 mL of TEOS was slowly added under a low agitation (350 rpm). After stirring for 15 min, the solution was held under an external magnetic field for 100 s. Finally, after standing for 12 h, the 1D $Fe_3O_4@SiO_2$ was synthesized by washing with deionized water and ethanol, and drying at 60 °C for 12 h.

Preparation of 1D yolk-shell Fe_3O_4@void@SnO_2: 0.1 g of the Fe_3O_4@SiO_2 was ultrasonically dispersed in a mixture of 12 mL H_2O and 18 mL anhydrous ethanol. Then, 0.9 g of urea and 0.12 g of $K_2SnO_3 \cdot 3H_2O$ were added to the above solution and stirred magnetically for 30 min, which was placed in an autoclave and kept in an oven at 170 °C for 6 h. At last, the Fe_3O_4@void@SnO_2 was obtained by washing several times with deionized water.

Preparation of Fe_2P@$SnP_{0.94}$: The Fe_2P@$SnP_{0.94}$ was prepared through a thermal phosphorization. Typically, 0.05 g of Fe_3O_4@void@SnO_2 and 1 g of $NaH_2PO_2 \cdot H_2O$ were mixed evenly. Then, the mixture was placed in a tubular furnace and calcined at 300 ℃ for 30 min under Ar gas at a ramping rate of 2 ℃ per min.

Preparation of ternary 1D Fe_2P@$SnP_{0.94}$@MoS_2: 0.05 g of Fe_2P@$SnP_{0.94}$, 0.154 g of $Na_2MoO_4 \cdot 2H_2O$, and 0.4 g of CH_4N_2S were stirred magnetically in 30 mL of H_2O for 30 min. Then, the above solution was transferred into an autoclave and kept in an oven at 190 °C for 16 h. After that, the sample was collected, washed and dried for further use.

Characterization: A field emission scanning electron microscopy (SEM, Hitachi S-4800), a transmission electron microscopy (TEM, HT-7700), and a X-ray diffractomerter (XRD, Bruker D8 Advance) were used to characterize the morphology and phase of the samples. The elemental mapping was tested on an energy dispersive X-ray spectrometer. The different valence states of the final product were detected by X-ray photoelectron spectroscopy tester (XPS, ESCALAB 250). Micrometritics ASAP 2460 analyzer was used to measure the specific surface area and pore-size distribution.

Electrochemical tests: The electrochemical properties of Fe_2P@$SnP_{0.94}$@MoS_2 were analyzed by using CR2032 coin cells, assembling in an Ar glove box (H_2O and O_2 < 0.01 ppm). The composite (65 w%), conductive carbon black (25 w%) and

carboxymethylcellulose (CMC,10 w%) in sodium carboxymethylcellulose (SBR) was evenly coated on a Cu foil, drying in a vacuum oven at 80 °C for 24 h, which was cut into a 12 mm-diameter disc. The electrolyte contained with 1 M of $LiPF_6$ in ethylene carbonate (EC) and ethyl methyl carbonate (EMC, volume ratio=1:1). Li metal was used as the counter electrode. The electrochemical performance of cells was tested on a CT-4008 system (Shenzhen Neware Technology Co., Ltd). An electrochemical workstation (CHI-660D) was used to measured cyclic voltammetry (CV) in the potential range of 0.01-3 V and electrochemical impedance spectra (EIS).

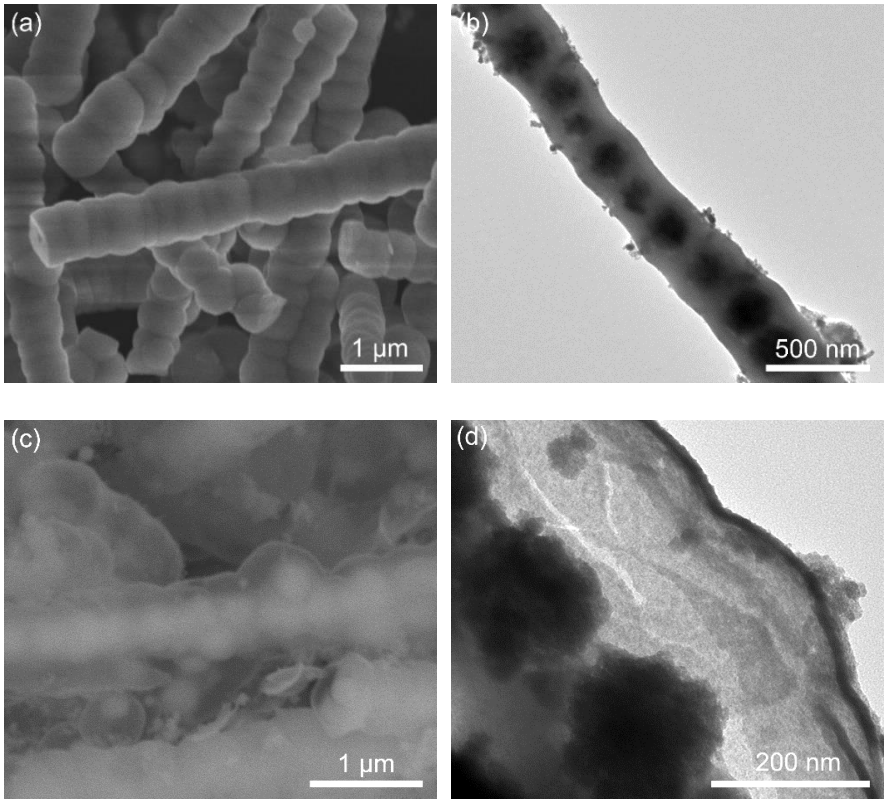

Fig. S1 (a) SEM and (b) TEM images of Fe_3O_4@SiO_2. (c) SEM and (d) TEM images of 1D Fe_3O_4@void@SnO_2.

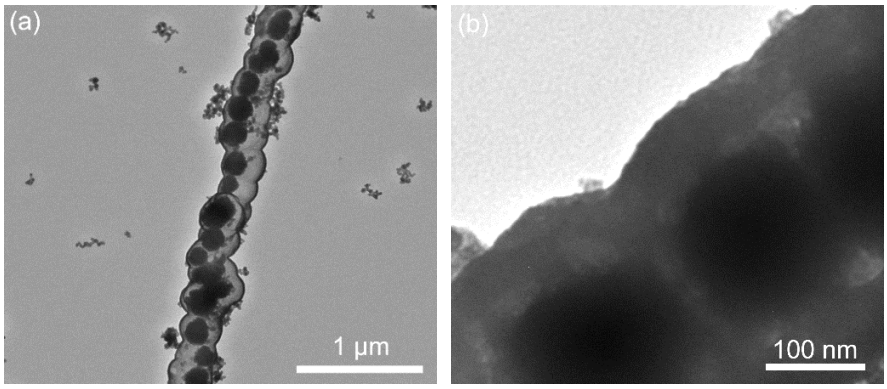

Fig. S2 (a,b) TEM images of the yolk-shell Fe_2P@void@$SnP_{0.94}$.

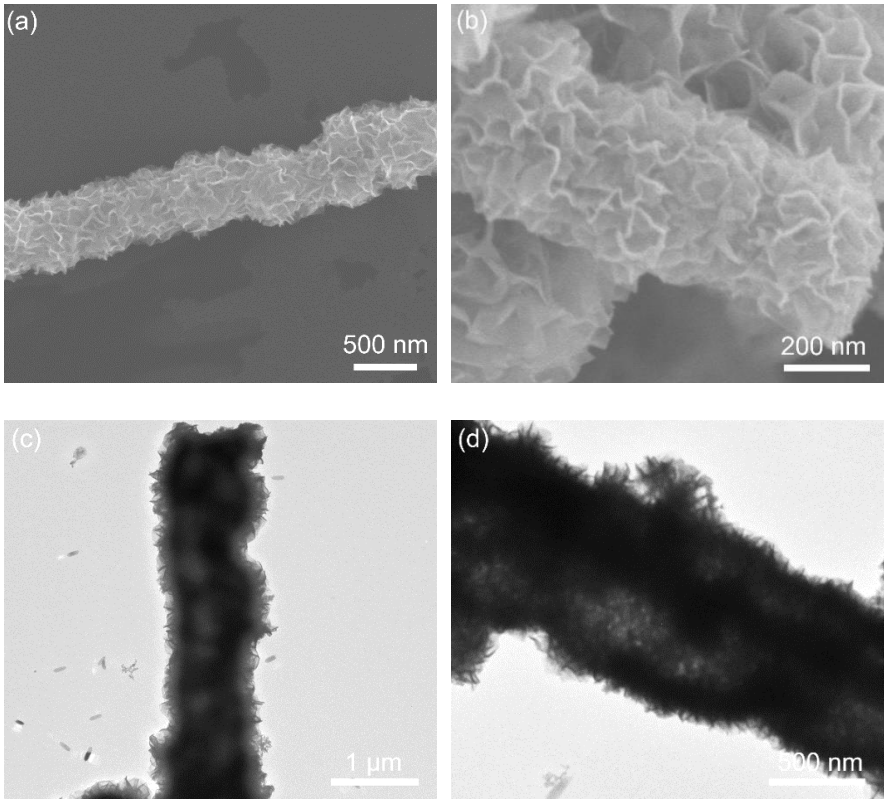

Fig. S3 (a,b) SEM and (c,d) TEM images of the Fe_2P@$SnP_{0.94}$@MoS_2.

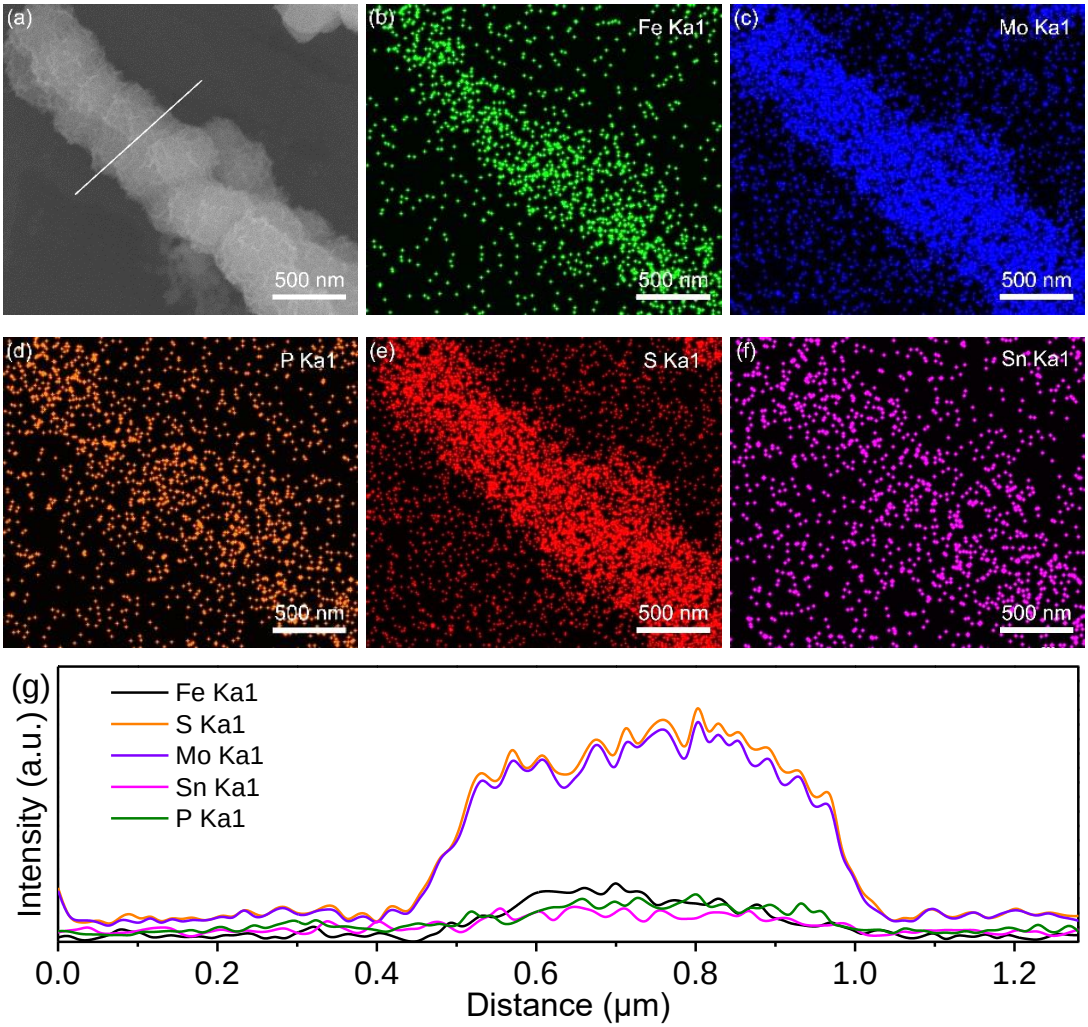

Fig. S4 (a) SEM and (b-f) mapping images of the $Fe_2P@SnP_{0.94}@MoS_2$ composite. (g) line-scanning curves.

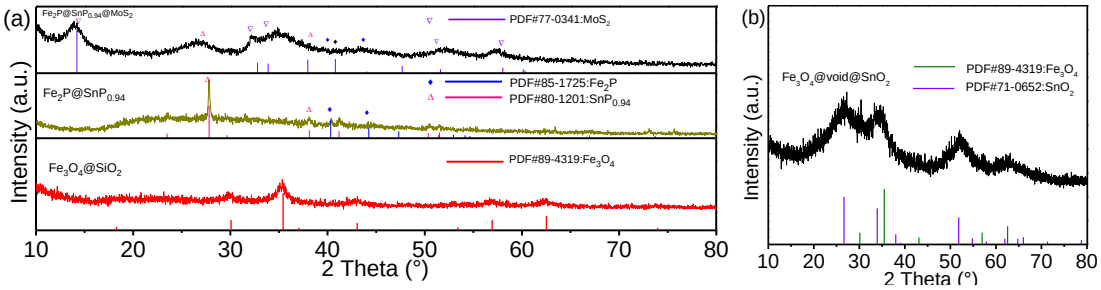

Fig. S5 (a, b) XRD patterns of each sample.

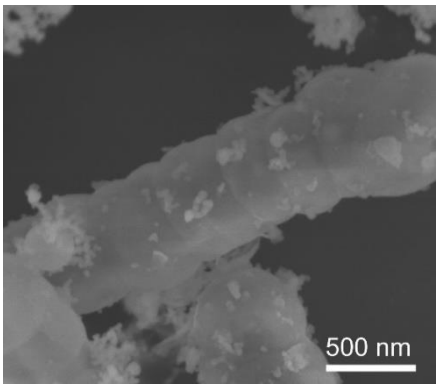

Fig. S6 SEM image of the Fe_2P@void@$SnP_{0.94}$.

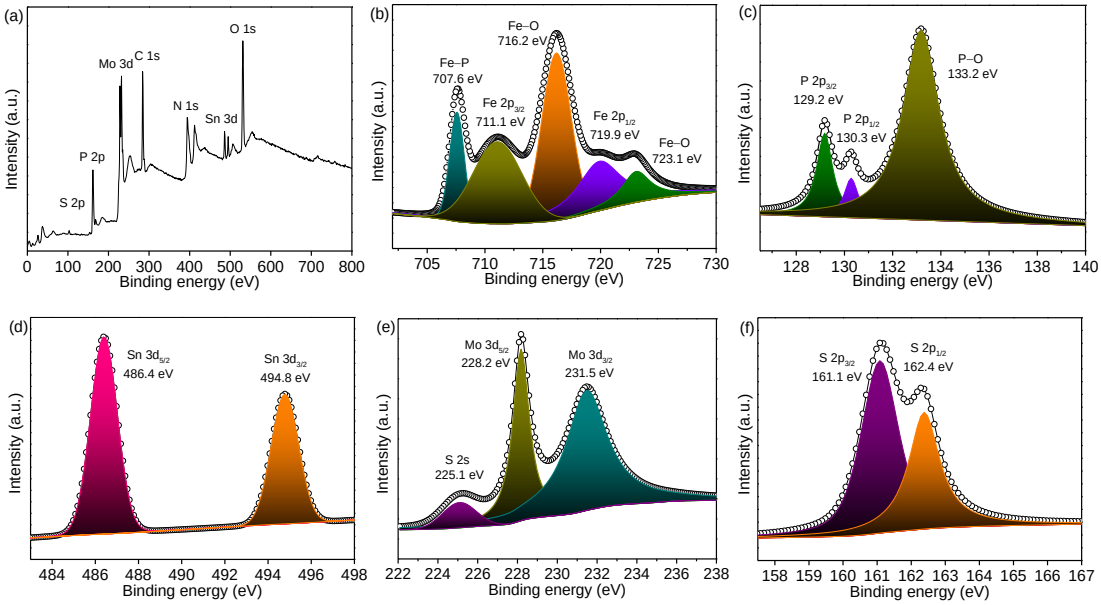

Fig. S7 (a) XPS spectra of Fe_2P@$SnP_{0.94}$@MoS_2: (a) survey spectrum, (b) Fe 2p, (c) P 2p, (d) Sn 3d, (e) Mo 3d, and (f) S 2p.

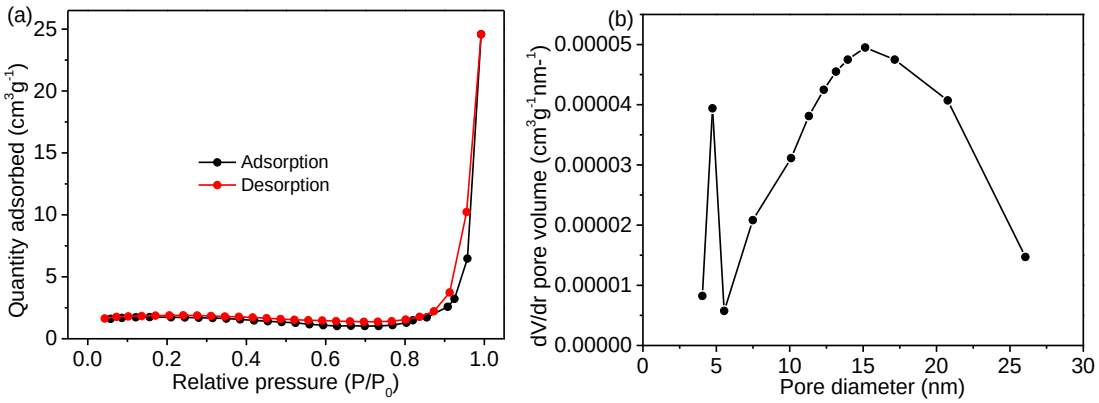

Fig. S8 (a) The N_2 adsorption-desorption isotherms of the composite. (b) The pore-size distribution.

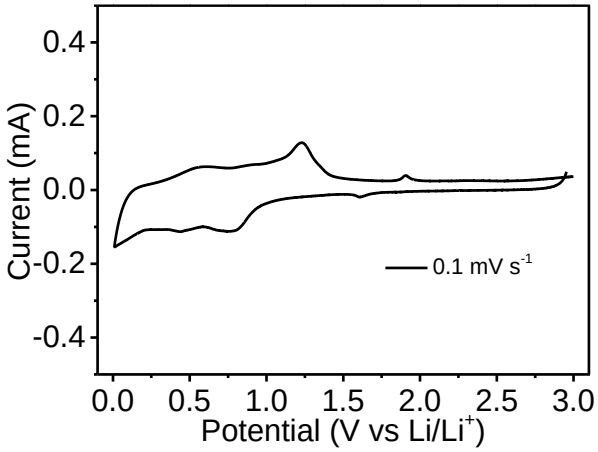

Fig. S9 CV curve of the $Fe_2P@SnP_{0.94}$ at a scanning speed of 0.1 mV s^{-1}.

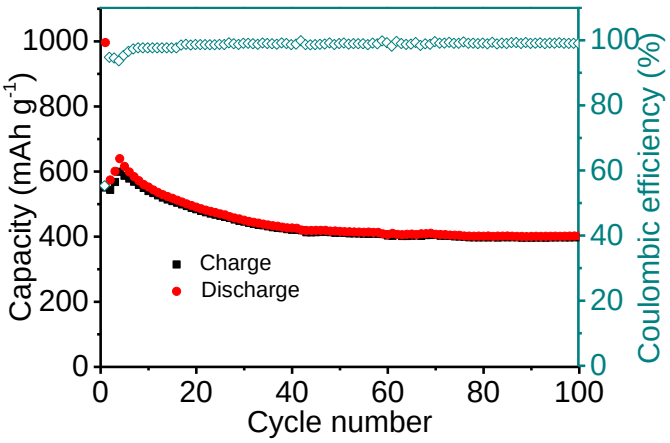

Fig. S10 Capacity and Coulombic efficiency of $Fe_2P@SnP_{0.94}$ cycling at 2 A g^{-1}.

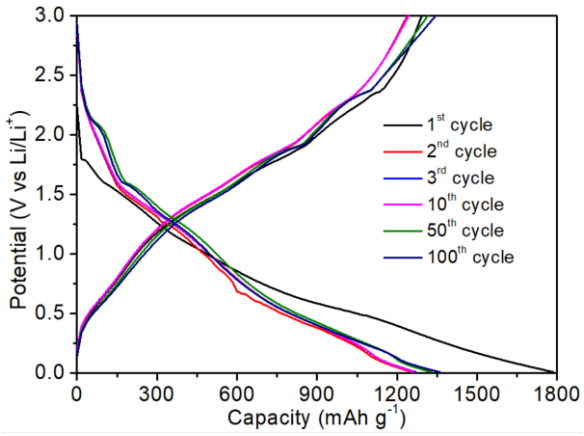

Fig. S11 (a) Charge-discharge profiles of the $Fe_2P@SnP_{0.94}@MoS_2$ composite cycling at 0.1 A g^{-1}.

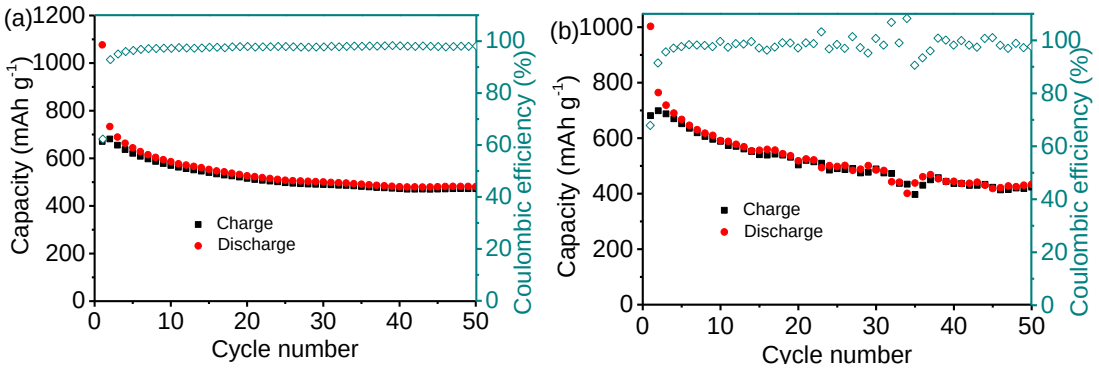

Fig. S12 Cycling performance and Coulombic efficiency of $Fe_2P@SnP_{0.94}$ at charge/discharge rates of (a) 0.5/1 A g^{-1} and (b) 1/0.5 A g^{-1}.

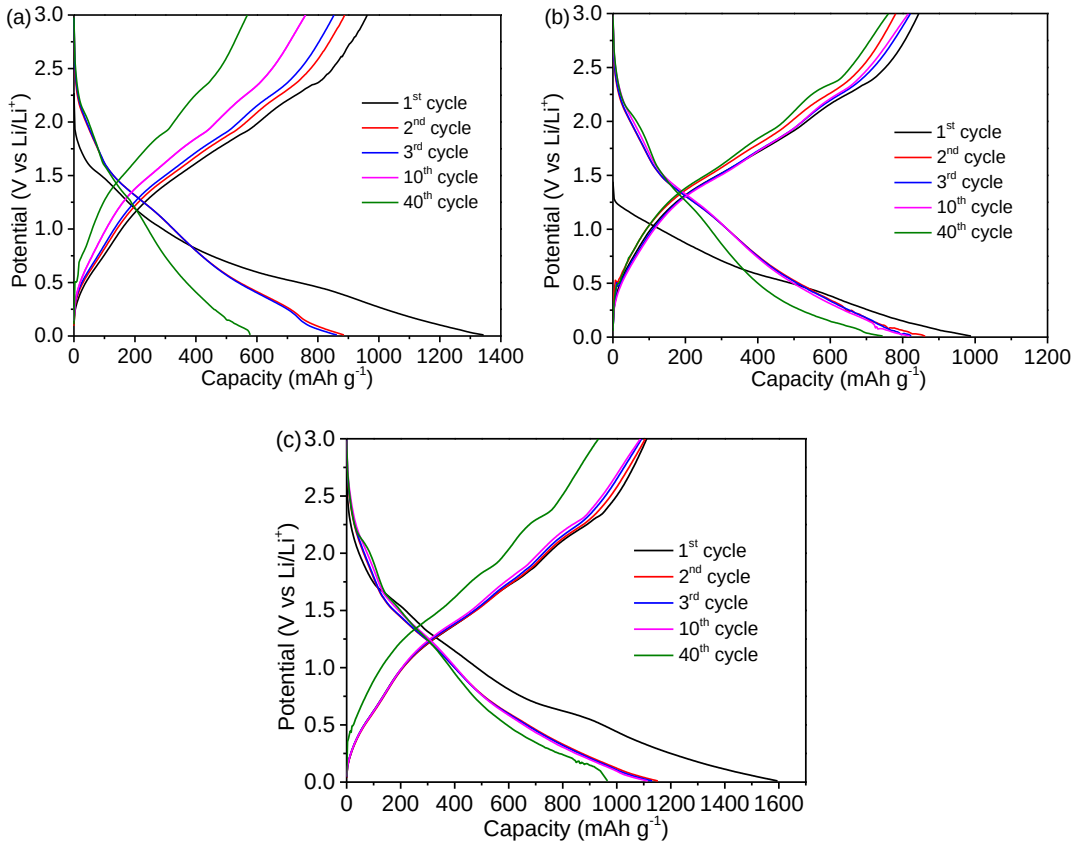

Fig. S13 Charge-discharge curves of the Fe_2P@$SnP_{0.94}$@MoS_2 composite cycling at 0.2 A g^{-1} under (a) –10 °C, (b) 25 °C, and (c) 45 °C.

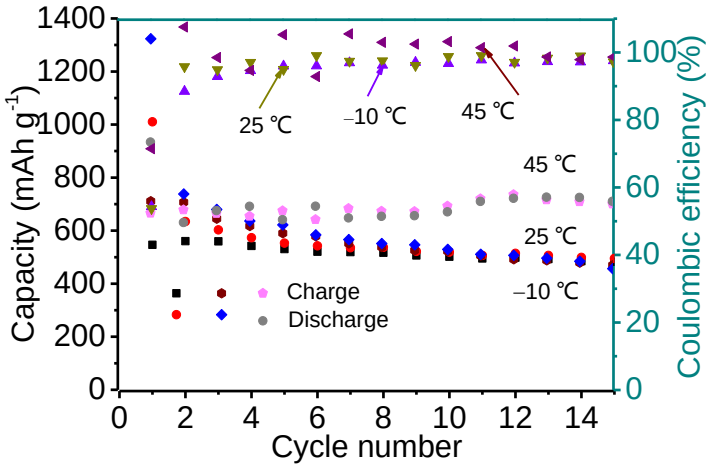

Fig. S14 Capacities and Coulombic efficiencies of Fe_2P@$SnP_{0.94}$ under –10 °C, 25 °C, and 45 °C when cycling at 0.2 A g^{-1}.

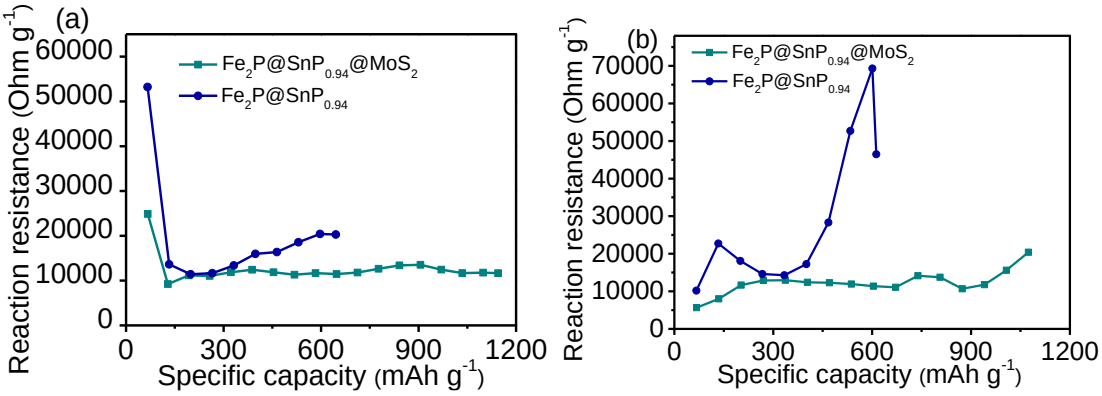

Fig. S15 *In-situ* reaction resistances at 0.2 A g^{-1}: (a) discharging and (b) charging.

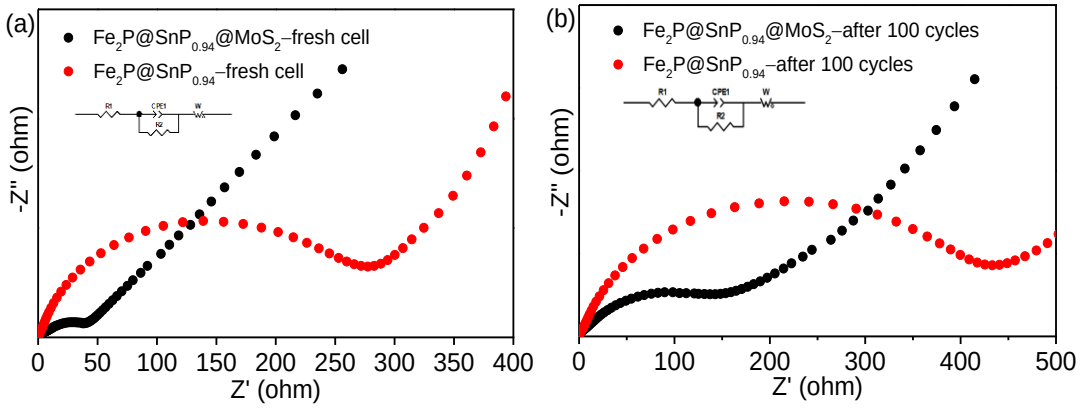

Fig. S16 EIS spectra of the $Fe_2P@SnP_{0.94}@MoS_2$ and $Fe_2P@SnP_{0.94}$ (a) before and (b) after 100 cycles at 2 A g^{-1}. The inserts display the equivalent circuits.

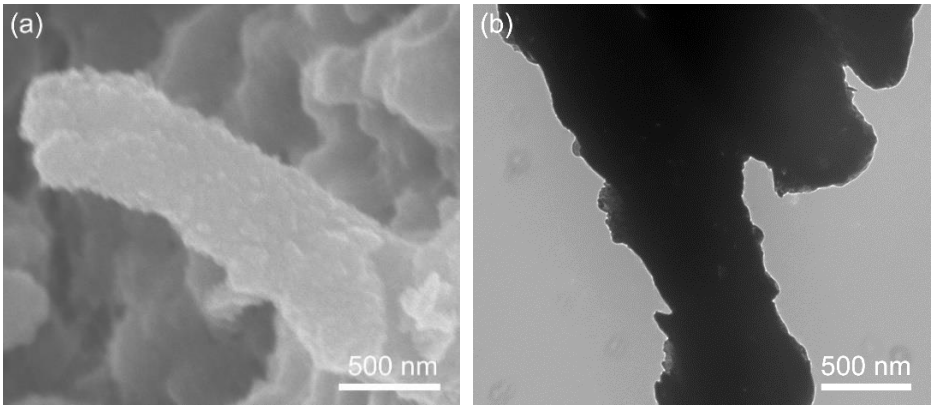

Fig. S17 (a) SEM and (b) TEM images of the $Fe_2P@SnP_{0.94}@MoS_2$ composite after cycling 100 times at 2 A g^{-1}.

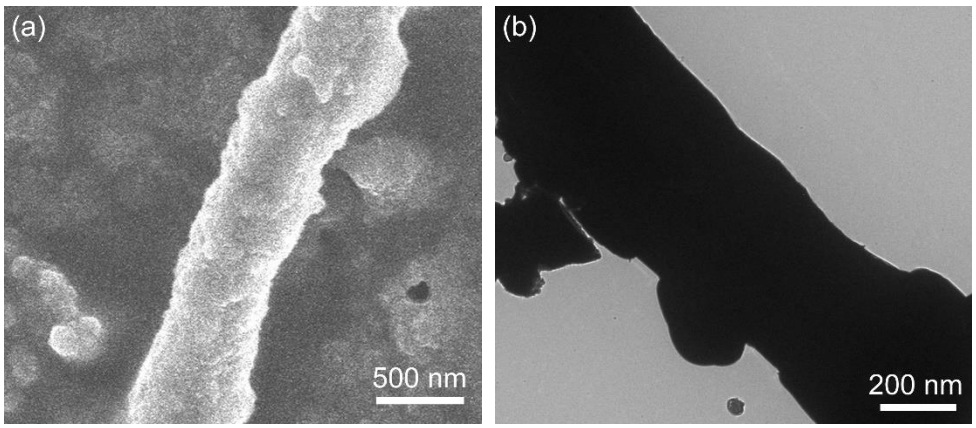

Fig. S18 (a) SEM and (b) TEM images of $Fe_2P@SnP_{0.94}$ after cycling 100 times at 2 A g^{-1}.

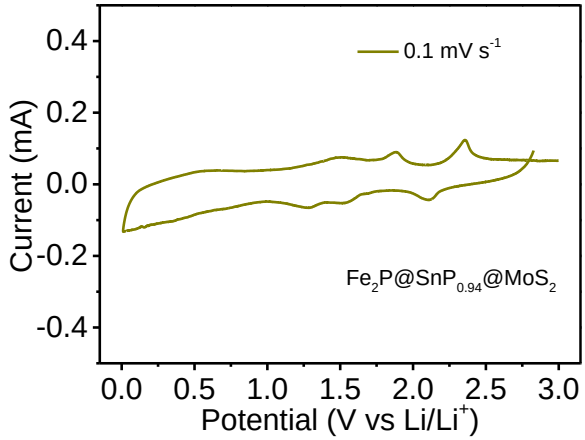

Fig. S19 CV profile of $Fe_2P@SnP_{0.94}@MoS_2$ at 0.1 mV s^{-1} after cycling 100 times at 2 A g^{-1}.

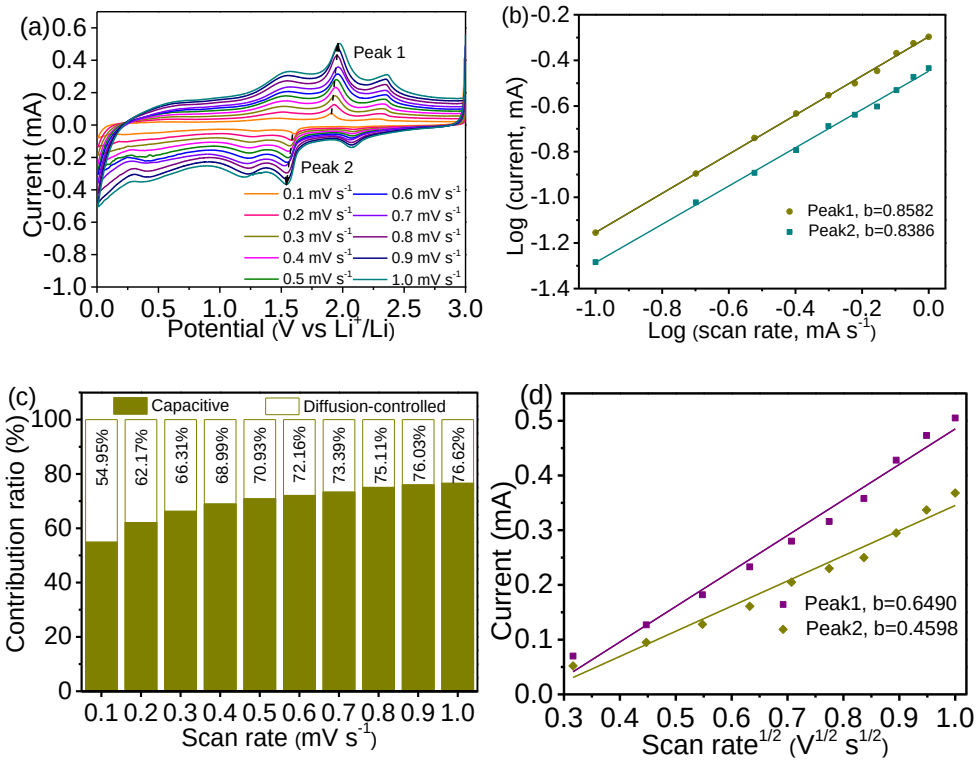

Fig. S20 (a) CV profiles at different scanning speeds from 0.1 to 1.0 mV s^{-1}. (b) Relationship of the log(*i*) *vs*. log(*v*). (c) Contribution ratios. (d) Peak currents *vs*. scan rate$^{1/2}$.

Table S1. Comparison on the electrochemical performance of some anodes.

Anode	Preparation method	Cycling rate (mA g^{-1})	Cycle number	Capacity (mAh g^{-1})	Ref.
Fe_2P/C composite nanofibers	Electrospinning	200	300	573	1
Butyl-capped Ge gels and $SnP_{0.94}$ nanoparticles	Vacuum annealing	440	200	500	2
Yolk–shell MoS_2 powders	Applying spray pyrolysis	1000	100	651	3
SnO_2/MoS_2	Hydrothermal method	1000	230	602	4
MoS_2@carbon	Hydrothermal method	2000	210	480	5
Graphene supported MoS_2 nanosheets	One-pot thermal annealing	150	50	1010	6
MoS_2@C	Hydrothermal method/carbonization	2000	500	530	7
Ternary 1D Fe_2P@$SnP_{0.94}$@MoS_2	Self-assembly and phosphorization	2000	800	797.5	This study

References

1 Y. Yang, W. B. Fu, C. Bell, D. C. Lee, M. Drexler, Y. Nuli, Z. F. M, A. Magasinski, G. Yushin and F. M. Alamgir, *ACS Appl. Mater. Interfaces,* 2021, **13**, 34074−34083.

2 M. G. Kim and J. Cho, *J. Electrochem. Soc.,* 2019, **156**, A277−A282.

3 Y. N. Ko, Y. C. Kang and S. B. Park, *Nanoscale,* **2014**, 6, 4508–4512.

4 Y. Chen, J. Lu, S. Wen, L. Lu and J. M Xue, *J. Mater. Chem. A,* 2014, **2**, 17857–17866.

5 R. Zhou, J. G. Wang, H. Z. Liu, H. Y. Liu, D. D. Jin, X. R. Liu, C. Shen, K. Y. Xie and B. Q. Wei, *Materials,* **2017**, 10, 174.

6 Q. H. Liu, Z. J. Wu, Z. L. Ma, S. Dou, J. H. Wu, L. Tao, X. Wang, C. B. Ouyang, A. L. Shen and S. Y. Wang, *Electrochim. Acta,* 2015, **177**, 298–303.

7 J. G. Wang, H. Y. Liu, R. Zhou, X. R. Liu and B.Q. Wei, *J. Power Sources,* 2019, **413**, 327–333.